Chapter 4 Synthesis of ZnO Nanowires on Polymer Substrate

4.1 Structural analysis

The ZnO NWs were hythermally grown on the ITO/PET and ZnO/ITO/PET substrates, and their corresponding FE-SEM images are shown in Fig. 4.1. The ZnO NWs grown on the ITO/PET substrate (Fig. 4.1(a)) has an uniform diameter of 50 nm, average length of 0.5 μm and an average number density of 1.2×10^{9} cm^{-2}. The surface morphology of ZnO NWs on ITO/PET substrate can be classified into two morphology types: one type is the ZnO NWs that aggregate to form the flower-like secondary particles region (region A) and another is the few randomly distributed NWs grown on part of the substrate (region B). Such a morphology variation is caused by the high lattice mismatch between ITO (a = b = c = 10.22 Å) and ZnO (a = b = 3.25 Å, c= 5.21 Å). The high lattice mismatch leads to be difficulty for the direct deposition of ZnO NWs on the ITO/PET substrate. Once ZnO grains are deposited on the substrate, the subsequent deposition of ZnO would be directed to the existing crystals. The type of nucleation results in forming the flower-like secondary particles. Thus, the ZnO NWs deposited on the ITO/PET substrate with the surface morphology of nonuniformity, random distribution and low number density. However, the surface morphology of the ZnO NWs on the ZnO/ITO/PET substrate is quite different. As shown in Fig. 4.1 (b), well-aligned ZnO NWs with hexagonal crystal structure grown on ZnO seeding layer have uniform diameter of 50 nm and number density of 3.4×10^{10} cm^{-2}. The cross sectional SEM image of ZnO NWs on the ZnO/ITO/PET substrate is shown in Fig. 4.1(c). The ZnO NWs were directly grown on the ZnO/ITO/PET substrate. The ZnO seeding film with the distinct orientation results in

the nonvertical random distribution of ZnO NWs. As a result, the surface morphologies of these hydrothermally grown ZnO NWs strongly depend upon the ZnO seeding layer.

Figure 4.2 shows the XRD patterns of PET, ZnO NWs/ITO/PET and ZnO NWs/ZnO/ITO/PET structures, respectively. The broad peaks at 53.8^{o} in the XRD patterns are caused by the PET substrate, and there is no ITO peaks observed in these samples since ITO films are too thin to be detected by the XRD. Single phase ZnO NWs could be synthesized on the ITO/PET and ZnO/ITO/PET substrates (Figs. 4.2(b) and (c)), respectively. The crystal structure of these NWs is wurtzite and no other phases appear. The lattice constants calculated from the XRD patterns of hydrothermally grown ZnO NWs are a = b = 3.25 Å and c = 5.21Å, which is consistent with that recorded in ICDD No. 80-0074. The ZnO NWs grown on the ZnO/ITO/PET exhibit the (002) preferred orientation, while the NWs on the ITO/PET show the (100) preferred orientation. The intensity of (100) peak of ZnO NWs/ITO/PET is identical to that of ZnO NWs/ZnO/ITO/PET, and the ratio of intensities (002) peak to (100) peak ($I_{(002)}/I_{(100)}$) of ZnO NWs/ITO/PET and ZnO NWs/ZnO/ITO/PET are 0.4 and 1.8, respectively. The preferred orientation and the ratio of peak intensity of NWs are related to the different surface morphologies (Fig. 4.1). The well-aligned ZnO NWs on the ZnO/ITO/PET substrate grow along the direction of [002] (can be observed from TEM results) which results in the (002) preferred orientation of the XRD pattern.

The HR-TEM images and the corresponding selected area electron diffraction (SAED) of high resolution region of hydrothermally grown ZnO NWs on ZnO/ITO/PET substrate are shown in Fig. 4.3, illustrating the morphology, growth orientation and crystal structure of the NWs. As indicated in Fig. 4.3(a), the ZnO NW grown uniformly along [002] direction with a diameter of 40 nm and length of 0.3 μm.

The SAED pattern which was indexed in Fig. 4.3(b) shows that the ZnO nanowire is single crystalline with the wurtzite structure. The lattice constants calculated from the indexed pattern are a = b = 3.25 Å and c = 5.21 Å, which are consistent with those calculated from the XRD result. In Fig. 4.3 (c), the ZnO NWs exhibit growth in the direction of [002] and the distance between parallel [002] lattice fringes of the ZnO NW is 5.21 Å. Thus, the single crystalline hydrothermally grown ZnO NWs are in the [002] orientation.

Room temperature transmission spectra of ITO/PET, ZnO NWs /ITO/PET and ZnO NWs/ZnO/ITO/PET were recorded by a UV–visible spectrometer, respectively. As shown in the Fig. 4.4, the transmittance of ITO/PET substrate is about 87 % under the range from 400 to 600 nm and the UV light with a wavelength smaller than 310 nm is absorbed by the PET substrate. As the ZnO NWs are grown on the ITO/PET and ZnO/ITO/PET substrates, the transmittances reduce to 78 and 53 %, respectively, under the range from 400 to 600 nm and the UV light is absorbed by these two samples. The transmittance of ZnO NWs/ZnO/ITO/PET is lower than that of the ZnO NWs/ITO/PET as the well-aligned ZnO NWs with high number density on ZnO/ITO/PET scatters and/or absorbs a part of the light that causes its transmittance decreases. The transmittance of ZnO NWs/ITO/PET is higher because of the nonuniform distribution and low number density of NWs. Two absorption steps could be observed in these samples since the first absorption edge of PET located at 310 nm and the second absorption edge resulting from the ZnO located at about 360 to 380 nm. To realize the relationship between the transmission spectra and the band gap, the absorption coefficient, α, is calculated after considering the reflection loss of the ITO/PET substrate and α^2 is plotted as a function of photon energy (hv) as shown in the inset of Fig. 4.4, which is used to determine the energy band gap (E_g) of ZnO NWs. As shown in the figure, two edges are observed; the edge at 3.8 eV is induced

by the PET substrate and that at 3.21 eV by the ZnO NWs. The band gap of ZnO NWs synthesized by hydrothermal method is slightly smaller than the value reported in the previous study[136]. This difference may be due to the nonstoichiometry and defects (proved in the following paragraph) of the hydrothermally grown ZnO NWs.

Figure 4.5 shows the photoluminescence spectra of ITO/PET substrate, flower-like ZnO NWs on the ITO/PET substrates and well-aligned ones on the ZnO/ITO/PET substrate. The optical properties were measured under a Xe lamp (λ = 325 nm) at room temperature. As shown in Fig. 4.5, the emission peak of the ITO/PET substrate is weak, and the locations of emitting peaks of ZnO NWs are independent of the substrate. The influence of different substrate is only on the intensity of the emission. Both of the ZnO NWs emit a strong emission at 406 nm (3.05 eV), luminescence at 465 nm (2.66 eV), 495 nm (2.52 eV) and 520 nm (2.38 eV). The UV emission is due to band-edge emission of ZnO. The band-edge emission intensity of ZnO NWs deposited on the ZnO/ITO/PET is higher than that on the ITO/PET substrate. It is suggested that the high number density of well-aligned ZnO NWs on the ZnO/ITO/PET substrate provides parallel laser cavities which can enhance the UV emission. On the contrary, the randomly distributed ZnO NWs on the ITO/PET substrate might scatter the emission of light that results in the weaker optical intensity. Moreover, there are emissions located at 450, 465, 495 and 520 nm for the hydrothermally grown ZnO NWs. The luminescences at 450, 465, 495 and 520 nm for ZnO were reported to be caused by the Zn–vacancy[185], oxygen–deficiency[186], deep–level[187] and singly ionized oxygen vacancies[188], respectively. These defects are caused by the growth environment of hydrothermally grown ZnO NWs. In the aqueous solution, the following reactions take place:

$$(CH_2)_6N_4+10\ H_2O \rightarrow NH_4OH+6\ HCHO \qquad [4.1]$$

$$Zn^{2+}+2\ OH^- \rightarrow ZnO+H_2O \qquad [4.2]$$

The OH^- ions are finite in the solution we used since the HMTA releases OH^- slowly, but Zn^{2+} ions are sufficient in this environment. Therefore, oxygen is expected to be lacking in the ZnO NWs fabricated by the hydrothermal method, which would lead to oxygen vacancies formation.

4.2 Electrical characterization

The field emission characteristics of the ZnO NWs on the ITO/PET and ZnO/ITO/PET substrates are indicated in Fig. 4.6. In Fig. 4.6(a), the ZnO NWs on the ITO/PET substrate exhibit the better field emission property. The turn on electric field (E_{on} defined as the electric field under 1.0 μA/cm^2) and threshold electric field (E_{th} defined as the electric field under 1.0 mA/cm^2) of flower like ZnO NWs on the ITO/PET substrate are 1.1 and 1.6 V/μm, respectively. As the ZnO NWs deposited on the ZnO/ITO/PET substrate, the E_{on} and E_{th} increase to 1.4 and 2.1 V/μm, respectively. The Fowler–Nordheim (F–N) plots for flower-like and well-aligned ZnO NWs respective on ITO/PET and ZnO/ITO/PET substrates are shown in the Fig. 4.6 (b), indicating that the field emission properties fit to the F–N relationship:

$$J = \frac{A\beta^2 E^2}{\phi}\exp\left(\frac{-B\phi^{3/2}}{\beta E}\right) \qquad [4.3]$$

where J is the current density (A/cm^2), E the applied field (V/μm), ϕ the work function of the emitter (ZnO, 5.37 eV[140]), β the field enhancement factor, $A = 1.56\times10^{-10}$ (AeVV^{-2}) and $B = 6.83\times10^{3}$ (VeV$^{-3/2}$ μm^{-1}). The β values of ZnO NWs on the ITO/PET and ZnO/ITO/PET substrates calculated from the slopes of the F–N plots are 4503 and 3340, respectively. It is well known that the β value depends on the geometry, structure, tip size and number density of the emitters on the substrate. The β

value of flower-like ZnO NWs is larger than that of well-aligned ZnO NWs. This phenomenon can be explained that a low number density and larger tip interspaces for the flower-like ZnO NWs on the ITO/PET substrate can reduce the screen effects, and consequently provide the low threshold electric field and larger β value.

The semi-logarithmic plots of J–E field emission characteristics shown in Fig. 4.6(c) demonstrate the emission properties further. The J-E curves can be divided into three parts: zero emission (region 1), F–N field emission (region 2) and current saturation regions (region 3). The turn on electric field, $E_{on,}$ is defined as the electric field for which tunneling occurs. The E_{on} of ZnO NWs on the ITO/PET substrate is 1.1 V/μm which is lower than that of ZnO NWs on the ZnO/ITO/PET substrate (1.4 V/μm). Above E_{on} (region 2), the emission current density increases abruptly and slows down at the high electric field region (region 3). A knee electric field, E_{knee}, is defined as the demarcation point between F–N field emission and current saturation regions. The E_{knee} of ZnO NWs on ITO/PET and ZnO/ITO/PET substrates are 1.6 and 2.0 V/μm, respectively. It has been reported that the saturation characteristics of field emission are caused by the high resistance in series of semiconductor emitters[189]. The resistances in series are introduced to fit the F-N saturating region to realize the conduction mechanism. The field emission characteristics are shown in Fig. 4.6 (c), and calculated resistance in series of ZnO NWs on the ITO/PET and ZnO/ITO/PET substrates are 55 and 82 kΩ, respectively. The increasing resistance in series may be contributed to the screen effect of the high number density of well-aligned ZnO NWs. Therefore, the current saturation region of ZnO NWs is owing to the effect of the high resistance of ZnO emitters. The flower-like ZnO NWs on the ITO/PET substrate with the low threshold electric field, high β value and low resistance in series are more suitable for the field emission applications.

The measurement of field emission properties of flower-like ZnO NWs

/ITO/PET under a 30 W incandescent lamp irradiation are carried out to realize the influence of the illumination on the field emission. The E_{on} and E_{th} decrease to 0.9 and 1.3 V/μm, respectively and the maximum current density increases to 18 mA/cm^2, as the flower-like ZnO NWs are illuminated. The calculated resistance in series of this sample under illumination from the fitting as shown in the insert of Fig. 3.7(a) is 43 kΩ. The β value (4510) of illuminated ZnO NWs on the ITO/PET substrates calculated from the slopes of the F–N plot (Fig. 4.7(b)) is close to that of dark one. Therefore, it is demonstrated that the carriers in the ZnO NWs are exciting during the illumination and increase the emission current density and reduce the resistance in series.

Based on the previous studies of our group[136,189], the vapor-liquid-solid (VLS) synthesized ZnO NWs with the higher aspect ratio and smaller tip diameter perform the better field emission characteristics (low threshold electric field, high current density and high β value). However, the hydrothermal method provides a low temperature process to fabricate the ZnO NWs. Consequently, the hydrothermal synthesized ZnO NWs are expected to be not only compatible to the Si-based microelectrics fabrication process but also to using the flexible polymer substrates for optoelectronic applications.

4.3 Conclusions

In conclusion, the single crystalline ZnO NWs are successfully grown on the flexible PET polymer substrates by hydrothermal route at 75 ^{o}C for 30 min.. The optical properties and field emission characteristics significantly depend on the surface morphologies of ZnO NWs deposited on the different substrates. The well-aligned ZnO NWs on ZnO/ITO/PET substrate perform the high band edge

emission due to the parallel laser cavities; while the flower-like ZnO NWs on ITO/PET substrate show the high transmission and better field emission abilities owing to the screen effect reduced by the low number density of NWs. The photoenhanced field emission properties are also observed in the ZnO NWs/ITO/PET device since the carriers are excited by photons. Thus, the hydrothermally grown ZnO NWs on the polymer substrate provide a low temperature synthesis process that may be appropriate for fabricating flexible optoelectronic and field emission devices.

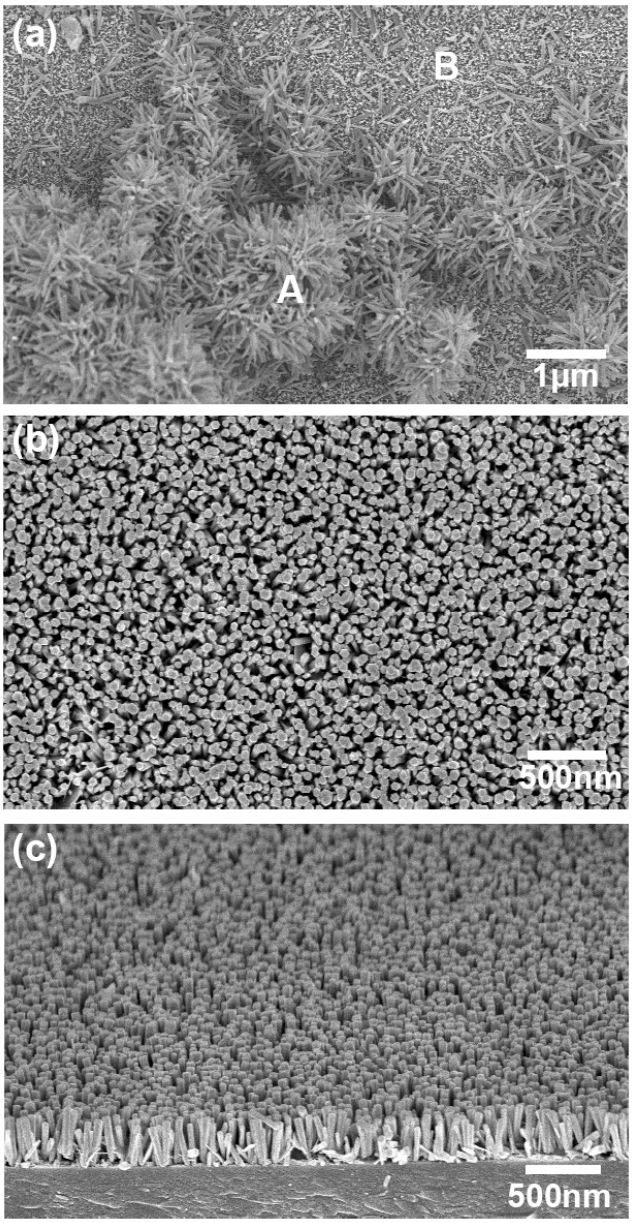

Figure 4.1 (a) FE–SEM micrographs of ZnO NWs on ITO/PET substrate. (b) FE–SEM micrographs of ZnO NWs on ZnO/ITO/PET substrate. (c) cross section FE–SEM image of ZnO NWs on ZnO/ITO/PET substrate.

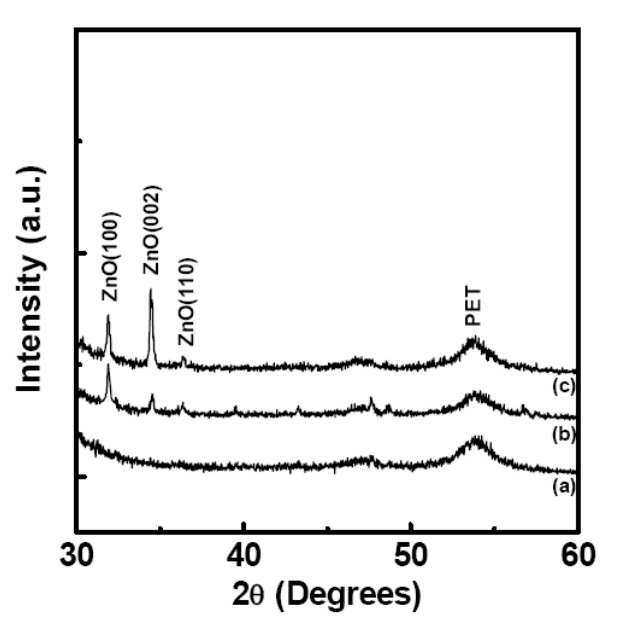

Figure 4.2 XRD patterns of (a) PET (b)ZnO NWs/ITO/PET, and (c) ZnO NWs/ZnO/ITO/PET.

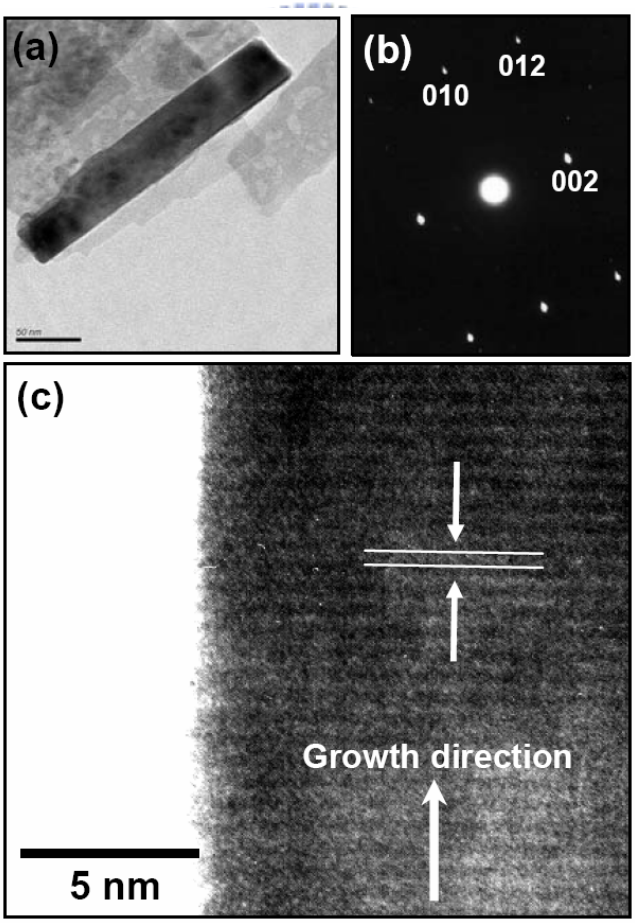

Figure 4.3 (a) TEM image of ZnO NW. (b) SAED of the high resolution region of ZnO NW. (c) HR–TEM image of ZnO NW.

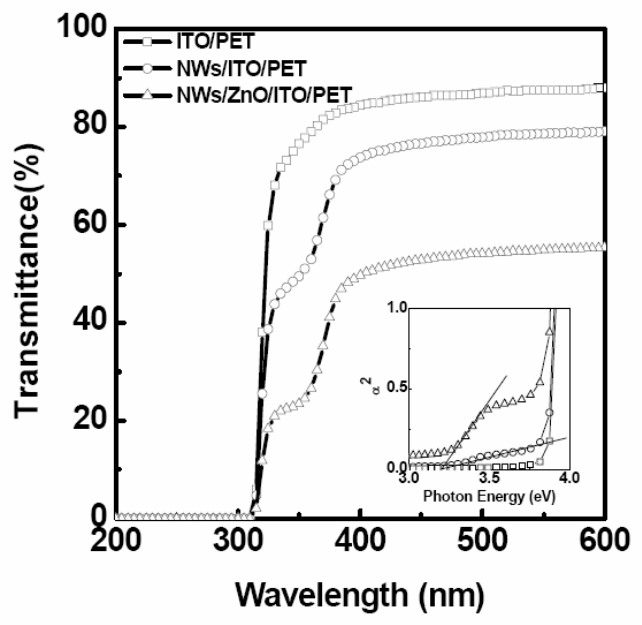

Figure 4.4 UV–VIS transmission spectra of ITO/PET, ZnO NWs/ITO/PET and ZnO NWs/ZnO/ITO/PET. The insert is the corresponding plot of α^2 vs. photon energy.

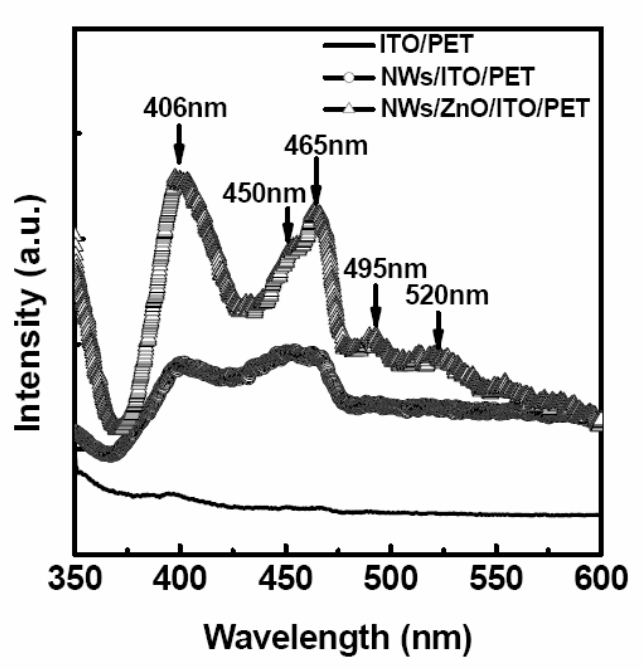

Figure 4.5 PL spectra of ITO/PET, ZnO NWs/ITO/PET and ZnO NWs/ZnO/ITO/PET.

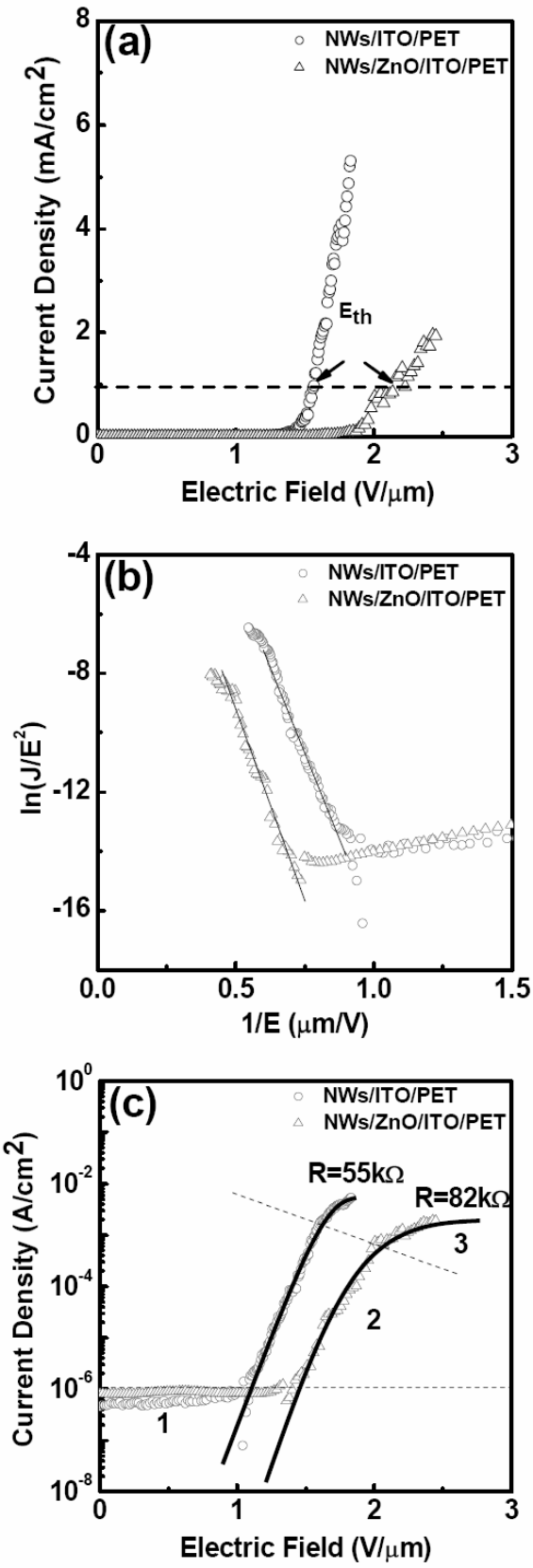

Figure 4.6 (a) Field emission current–voltage curves of ZnO NWs on the ITO/PET and ZnO/ITO/PET substrates. (b) The corresponding Fowler–Nordheim plots of NWs. (c) Semi- logarithmic plot of J–E field emission characteristics and the corresponding resistance in series fitting.

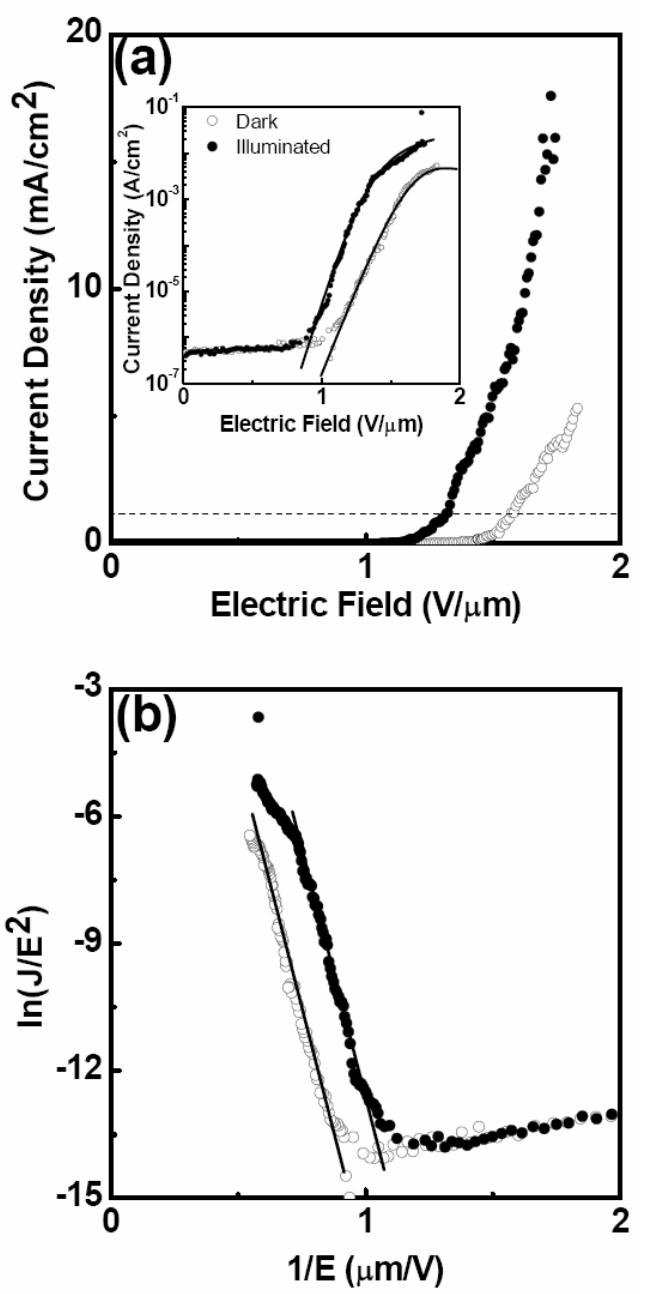

Figure 4.7 (a) Photoenhanced field emission characteristics of ZnO NWs on ZnO/ITO/PET substrates. The insert is the fitting of resistance in series (b) Corresponding F–N plots.